

PV Cell Orientation Angles Optimization for a Base Station Equipped with Several PV Cells

Doris Benda, *Student Member, IEEE*, Sumei Sun, *Fellow, IEEE*, Xiaoli Chu, *Senior Member, IEEE*, Tony Q.S. Quek, *Fellow, IEEE*, and Alastair Buckley

Abstract—We jointly optimize the orientation angles of N photovoltaic (PV) cells powering one base station (BS). There are more degrees of freedom for matching the energy generation profile of the PV cells to the energy consumption profile of the BS by deploying the PV cells with potentially different orientation angles. We derive analytically the energy generation profile of any randomly inclined and oriented PV cell from the irradiance values received at a horizontally mounted PV cell at the same location. The energy drawn per day from the main grid by the BS given its energy consumption profile is used as performance metric to determine the optimal set of orientation angles. Our results are that deploying one PV cell (or several PV cells) with the (same) optimized orientation angle is recommended for BSs with an energy consumption profile that has one significant local maximum between sunrise and sunset. Deploying two PV cells (or two equal-sized groups of PV cells) where the two orientation angles (of the two groups) are jointly optimized is recommended for BSs with an energy consumption profile that has significant local maxima in the morning as well as in the afternoon or with a constant energy consumption profile.

Index Terms—Cellular networks, solar powered, PV cells, orientation angle, inclination angle, base stations

I. INTRODUCTION

A. Background

Dense deployment of base stations (BSs) is necessary to meet the increasing traffic demand of new applications, such as ultra high definition video streaming, autonomous driving, and virtual reality based applications [1]. As a consequence, the accumulated BS energy consumption is rising considerably. To alleviate the impact on the environment and the cost burden on cellular network operators, photovoltaic (PV) cell powered BSs have been considered for future cellular networks [2], [3].

Manuscript received #####; revised #####. This work was supported by the A*STAR-Sheffield Research Attachment Programme. This work was partly funded by the European Unions Horizon 2020 Research and Innovation Programme under grant agreement No 645705 and by the A*STAR Industrial Internet of Things Research Program, under the RIE2020 IAF-PP Grant A1788a0023.

D. Benda is with the Department of Electronic and Electrical Engineering, University of Sheffield, Sheffield S1 4ET, U.K., and also with the Communications and Networks Cluster, Institute for Infocomm Research, Singapore 138632 (e-mail: dcbenda1@sheffield.ac.uk).

S. Sun is with the Communications and Networks Cluster, Institute for Infocomm Research, Singapore 138632 (e-mail: sunsm@i2r.a-star.edu.sg).

X. Chu is with the Department of Electronic and Electrical Engineering, University of Sheffield, Sheffield S1 4ET, U.K. (e-mail: x.chu@sheffield.ac.uk).

T. Q. S. Quek is with the Information Systems Technology and Design Pillar, Singapore University of Technology and Design, Singapore 487372 (e-mail: tonyquek@sutd.edu.sg).

A. Buckley is with the Department of Physics and Astronomy, University of Sheffield, Sheffield S3 7RH, U.K. (e-mail: alastair.buckley@sheffield.ac.uk).

The energy generation profiles of the PV cells do not match the energy consumption profile of the appliance in general. The most common solutions to this problem reported in the literature are either energy storage technologies or demand side management [4]. Supply side management has not been sufficiently studied. In this paper, we derive a methodology to adjust the solar energy supply to meet the energy demand of the BS in the time domain.

B. PV Cell Angles

As shown in Fig. 1, the inclination angle of a PV cell, denoted by γ , is defined as the angle between the horizontal plane and the PV cell plane, whereas the orientation angle of a PV cell, denoted by θ , is defined with respect to the southern direction. For instance, the orientation angles of a PV cell orientated towards the east, south, and west are $\theta = -90^\circ$, $\theta = 0^\circ$, and $\theta = 90^\circ$, respectively.

The daily energy generation profile of a PV cell depends on the day of the year, the deployment location, the orientation angle θ , and the inclination angle γ of the PV cell.

The orientation and inclination angles of PV cells are usually fixed after the initial installation. Therefore, it is necessary to optimize the orientation and inclination angles of PV cells prior to the deployment. Without considering the energy consumption profile of the appliance, PV cells are deployed with default angles that are derived from the PV cell's geographic location as summarized in Table I. The default inclination angle is set at a value similar to the latitude of the deployment area, and the default orientation angle is 0° , and 180° in the northern, and southern hemispheres, respectively [5]. These default angles guarantee that the PV cells harvest the most energy on a yearly timescale among all possible orientation and inclination angles.

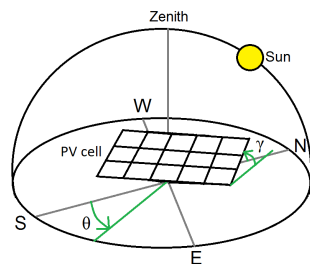


Figure 1: Depiction of a PV cell installed with the orientation angle $\theta = -30^\circ$ and with the inclination angle $\gamma = 20^\circ$

Table I:
DEFAULT OPTIMAL ORIENTATION ANGLE θ AND INCLINATION ANGLE γ
FOR DIFFERENT LOCATIONS [5]

| Location | θ | γ |
|---------------------|-----------------------|------------------------------------|
| Northern hemisphere | 0° | similar to the location's latitude |
| Southern hemisphere | 180° | similar to the location's latitude |
| Equator | any orientation angle | 0° |

In general, optimizing the PV cell inclination angle is done on a yearly timescale because it is a method to shift the energy generation peak from a surplus season (e.g. summer) to a deficit season (e.g. winter). In contrast, optimizing the PV cell orientation angle is done on a daily timescale because it is a method to shift the energy generation peak from a surplus time (e.g. noon) to a deficit time (e.g. morning or afternoon).

Fig. 2 shows the daily energy generation profile of southeast, south, and southwest-oriented PV cells, which are denoted by $G_{-45^\circ,1}(t)$, $G_{0^\circ,1}(t)$, and $G_{45^\circ,1}(t)$, respectively, for London during the summer. Orientating a PV cell eastwards (westwards) shifts the energy generation profile towards the morning (afternoon) hours in the northern hemisphere. The farther a PV cell is oriented away from the southern direction the less energy it harvests throughout the whole day.

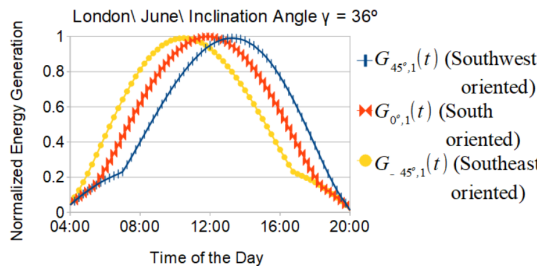


Figure 2: Effects of the orientation angle θ on the PV cell energy generation profile

C. Literature Review

Most papers investigating differently oriented PV cells, such as [6], have not actually optimized the PV cell angles but considered some deployment constraints, e.g., that the PV cells are mounted on residential rooftops, which predefine the PV cell angles. Paper [7] determined the optimal building orientation that minimizes the cooling demand of the building by reducing the irradiance on the building.

PV cell angle optimization for maximizing the total energy output of the PV cells have been done for Singapore in [8], however, without considering the potential mismatch between the energy generation profile of the PV cells and the energy consumption profile of the appliance. This may result in service outage if the PV cells are the only energy source or additional expenditures if the energy deficit has to be compensated by using alternative energy sources.

In [9], the PV cell angle optimization considered the energy demand of the Ontario province of Canada, where the authors

investigated orientation angles between 15° east of due south to 15° west of due south, i.e., $\theta \in [-15^\circ, 15^\circ]$. In addition, propagation losses along the power lines among the widely-distributed PV cell installations were not included, which are significant factors when operating on a provincial scale [10], [11].

The authors of [12] investigated five orientation angle settings (east, southeast, south, southwest, and west) and concluded that in some scenarios a mix of east-oriented and west-oriented PV cells and in other scenarios south-oriented PV cells reduce the needs for storage and backup from dispatchable energy sources in a fully renewable European power system. Because they adjusted the installed capacity of the PV cells for each angle configuration, such that the average power production of each PV cell remains the same, it is difficult to fairly judge if the reduced needs for storage and backup are a good trade-off for the increased installed capacity of PV cells.

Optimizing the PV cell inclination angle to power an isolated island was studied in [13], where the PV cell inclination angle was optimized on a yearly timescale. Because the PV cell inclination angle was optimized, the energy can be shifted on a yearly timescale, i.e., from a surplus season (e.g. summer) to a deficit season (e.g. winter), but the energy cannot be shifted on a daily timescale, i.e., from a surplus time (e.g. noon) to a deficit time (e.g. morning or afternoon) with the proposed method in [13].

Optimizing the PV cell orientation angle of only one PV cell deployed at the BS to match the energy generation of this single PV cell with the energy consumption of a BS has been studied in our previous works [14]–[16].

D. Contributions

In this paper, we focus on orientation angle optimization on a daily timescale. Different from [9], we optimize the PV cell orientation angles in the range from east ($\theta = -90^\circ$) to west ($\theta = 90^\circ$) to match a given energy consumption profile rather than maximizing the total energy output of the PV cells. Different from [12], we keep the installed capacity of the PV cells unchanged in our system model. Hence, it is possible to fairly present the improvement caused by different PV cell orientation angles. Different from [14]–[16], we consider several potentially differently oriented PV cells and investigate how the number of PV cells and composition of differently oriented PV cells improve the match between the energy generation profile of the PV cells and the energy consumption profile of the BS.

The main contributions of this paper can be summarized as follows:

- We jointly optimize the orientation angles of several PV cells powering one BS.
- We derive analytically the irradiance values on any randomly inclined and oriented PV cell. Only the irradiance values of a horizontally mounted PV cell have to be given for our method as the baseline.

- We analytically identify and discuss to what extent the orientation angle θ shifts the energy generation profile away from noon if the PV cells are not south-oriented ($\theta \neq 0^\circ$).
- We evaluate the effectiveness of our proposed orientation angle optimization on three different types of BS energy consumption profiles: constant traffic load profiles, business-area traffic load profiles, and residential-area traffic load profiles. The energy drawn from the main grid by the BS per day is used as the performance metric.
- The proposed optimization only needs to run a single time offline and the obtained optimal angles can be used for all solar-powered BSs with similar geographic locations and energy consumption profiles.
- We give recommendations on how many differently oriented PV cells should be deployed for a given energy consumption profile. To the best of our knowledge, this has never been investigated in the literature.

The rest of this paper is organized as follows: The system model is presented in Section II and consists of the energy generation model, the ground-reflected irradiance model, the direct-beam irradiance model, the sky-diffuse irradiance model, the energy consumption model, and the objective function. To what extent the orientation angle θ determines the position in time of the peak of the energy generation profile is discussed in Section III. The numerical results and the key findings are presented in Section IV. Finally, our recommendations and our concluding remarks are given in Section V.

II. SYSTEM MODEL

All angles in this paper are in degrees. Fig. 3 depicts the system model considered in this paper. The energy generation part consists of N identical PV cells, denoted by PV cell 1, PV cell 2, ..., and PV cell N , $N \in \mathbb{N}$. The energy consumption part consists of a BS. The total surface area of all N PV cells is A . Each PV cell has a surface area of $\frac{A}{N}$. The day is divided into T time steps, $T \in \mathbb{N}$. The index of a time step is denoted as t , $t \in \{1, \dots, T\}$. The BS uses the energy generated by the N PV cells, denoted by $G(t)$, to support its energy consumption $C(t)$ at every time step t . If there is an energy deficit, i.e., $C(t) - G(t) > 0$, the BS draws the remaining energy from the main grid at time step t . If there is an energy surplus, i.e., $C(t) - G(t) < 0$, the surplus energy is wasted at time step t ¹.

¹This assumption is justified because most power grids nowadays are still designed for one-directional energy flow from a few large-scale centralized energy generators, such as coal power plants or nuclear power plants, to many small-scale energy consumers, such as domestic households or BSs. Current power grid infrastructure is often not assigned to accommodate huge amounts of energy flow in opposite direction and to redistribute such intermittent generated energy sufficiently without causing grid instability or jeopardizing the reliability of the power grid. Even if surplus energy can be sold to the grid, our system model aims to match the energy generation profile with the energy consumption profile on-site at a BS, which is more cost-effective for the BS/PV cells owner than wasting the surplus energy or selling the surplus energy to the grid for redistribution. Grid operators always sell energy at a higher price than they buy it. In addition, matching the energy generation profile with the energy consumption profile on-site at a BS reduces the stress on the power grid.

The optimization object in our system model is to minimize the amount of energy that has to be drawn from the main grid by the BS on a daily time scale. The energy drawn from the main grid can only be altered by choosing different orientation angles $\theta_1, \dots, \theta_N$ for PV cell 1, ..., and PV cell N , respectively. All the other parameters of the system, including the inclination angles of all N PV cells, are fixed. In this paper, we use a system located in Greenwich (London, UK) as example, i.e., the Latitude lat , and the Longitude lon are fixed to 51.4767° North, and 0.0003° West, respectively, but the analysis can be applied to other locations as well. Hence, all formulas in this paper are given for a location in the northern hemisphere.

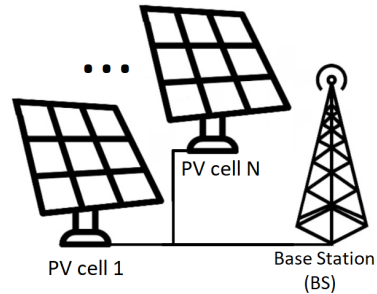


Figure 3: System model

A. Energy Generation

We use a horizontally mounted PV cell in Greenwich (London, UK) as the baseline. From this baseline, we develop a method to calculate the energy generated by a PV cell at the same location but installed with any orientation angle $\theta \in [-90^\circ, 90^\circ]$ and any inclination angle $\gamma \in [0, 90^\circ]$. The global horizontal irradiance GHI_t , the diffuse horizontal irradiance DHI_t , and the direct normal irradiance DNI_t for a horizontally mounted PV cell in Greenwich (London, UK) are obtained from the PVGIS database (cf. Fig. 4) for every time step t . GHI_t , DHI_t , and DNI_t , are fixed values that we can use in the following sections for every time step t .

Denote $G_{\theta,N}^{\text{original}}(t)$ as the energy generated by one PV cell installed with orientation angle θ and surface area $\frac{A}{N}$. It can be calculated by

$$G_{\theta,N}^{\text{original}}(t) = I_\theta(t) \cdot \eta \cdot \frac{A}{N} \cdot \bar{t}, \quad (1)$$

where $I_\theta(t)$ is the irradiance received by the PV cell, η is the energy conversion efficiency, $\frac{A}{N}$ is the surface area of the PV cell, and \bar{t} is the duration of one time step.

To facilitate a fair comparison in Section IV, we normalize all energy generation values with respect to a south-orientated PV cell in Greenwich at noon with surface area A . Hence, $G_{\theta,N}(t)$ is the normalized energy generated by one PV cell installed with orientation angle θ and can be calculated by

$$G_{\theta,N}(t) = \frac{G_{\theta,N}^{\text{original}}(t)}{G_{0^\circ,1}^{\text{original}}\left(\frac{T}{2}\right)} = \frac{I_\theta(t)}{I_{0^\circ}\left(\frac{T}{2}\right) \cdot N} = \frac{I_\theta(t)}{614 \frac{\text{W}}{\text{m}^2} \cdot N} \quad (2)$$

We obtain $G_{(\theta_1, \dots, \theta_N)}(t)$, which is the normalized energy generated by N PV cells, as follows:

$$G_{(\theta_1, \dots, \theta_N)}(t) = \sum_{i=1}^N G_{\theta_i, N}(t) \quad (3)$$

As a result, if all N PV cells are oriented to the south, they generate exactly 1 unit of energy at noon, i.e., $G_{(\theta_1, \dots, \theta_N)}\left(\frac{T}{2}\right) = G_{(0^\circ, \dots, 0^\circ)}\left(\frac{T}{2}\right) = 1$.

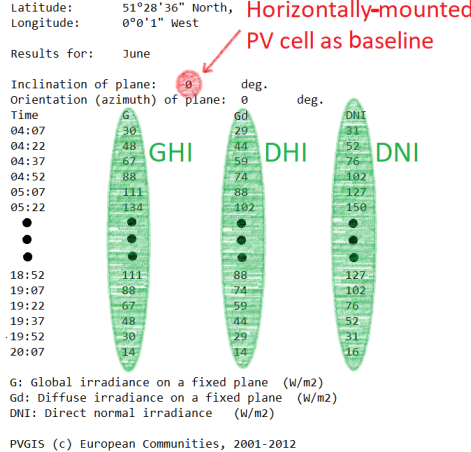


Figure 4: Data sheet downloaded from [17]

The irradiance $I_\theta(t)$ received by one PV cell installed with orientation angle θ at time step t can be calculated by [18] as follows:

$$I_\theta(t) = I_{b_\theta}(t) + I_{d_\theta}(t) + I_g(t), \quad (4)$$

where $I_{b_\theta}(t)$ is the direct-beam component, $I_{d_\theta}(t)$ is the sky-diffuse component, and $I_g(t)$ is the ground-reflected component. Fig. 5 shows the three components graphically. We investigate the three irradiance components in the next three sections separately.

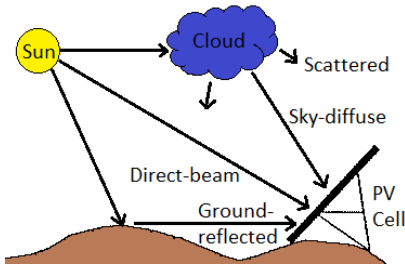


Figure 5: Irradiance model

B. Ground-Reflected Irradiance $I_g(t)$

The ground-reflected irradiance $I_g(t)$ is independent of the orientation angle θ and can be calculated by [19] as follows:

$$I_g(t) = GHI_t \cdot \alpha \cdot \frac{1 - \cos(\gamma)}{2}, \quad (5)$$

where $\alpha \in [0, 1]$ is the albedo of the ground. The albedo is dimensionless and measures the amount of sunlight that a

surface reflects. A black body that absorbs all sunlight has an albedo value of 0. A body that reflects all sunlight has an albedo value of 1. For example, snow has a high albedo and hence, appears bright. Trees have a low albedo and hence, appear dark.

C. Direct-Beam Irradiance $I_{b_\theta}(t)$

The direct-beam irradiance $I_{b_\theta}(t)$ depends on the orientation angle θ and can be calculated by [18] as follows:

$$I_{b_\theta}(t) = DNI_t \cdot \max(0, \cos(AOI_\theta(t))), \quad (6)$$

where $AOI_\theta(t)$ is the angle of incidence at time step t .

It is important to include the max in (6) to model that no energy can be harvested if the PV cell is illuminated from the back, i.e., $AOI_\theta(t) > 90^\circ$. For example, if the PV cell is oriented to the east then $AOI_\theta(t)$ will be greater than 90° in the evening. Hence, $\cos(AOI_\theta(t))$ will be smaller than 0. This will result in a negative irradiance value $I_{b_\theta}(t)$ during the evening, which makes no sense. As a result, the max in (6) is necessary.

The angle of incidence $AOI_\theta(t)$ is the angle between the line that points to the sun and the normal vector to the PV cell panel (cf. Fig. 7 (a)). $AOI_\theta(t)$ can be calculated by [20] as follows:

$$\begin{aligned} \cos(AOI_\theta(t)) = & + \sin(\delta_d) \sin(lat) \cos(\gamma) \\ & + \cos(\delta_d) \cos(lat) \cos(\gamma) \cos(\omega_t) \\ & + \cos(\delta_d) \sin(\gamma) \sin(\omega_t) \sin(\theta) \\ & - \sin(\delta_d) \cos(lat) \sin(\gamma) \cos(\theta) \\ & + \cos(\delta_d) \sin(lat) \sin(\gamma) \cos(\omega_t) \cos(\theta) \\ = & a_t + b_t \sin(\theta) + c_t \cos(\theta), \text{ with} \end{aligned} \quad (7)$$

$$a_t = + \sin(\delta_d) \sin(lat) \cos(\gamma) + \cos(\delta_d) \cos(lat) \cos(\gamma) \cos(\omega_t), \quad (8)$$

$$b_t = + \cos(\delta_d) \sin(\gamma) \sin(\omega_t), \quad (9)$$

$$c_t = - \sin(\delta_d) \cos(lat) \sin(\gamma) + \cos(\delta_d) \sin(lat) \sin(\gamma) \cos(\omega_t), \quad (10)$$

where lat is the latitude of the deployment area, δ_d is the declination angle, and ω_t is the hour angle at time step t . a_t , b_t , and c_t include the parts that are independent of θ , are multiplied by $\sin(\theta)$, and are multiplied by $\cos(\theta)$, respectively.

The declination angle δ_d can be calculated by [21] as follows:

$$\delta_d = 23.45^\circ \cdot \sin\left(\frac{360}{365}(d + 284)\right), \quad (11)$$

where d is the day of the year with 1st of January as $d = 1$.

The declination angle models the different seasons (cf. Fig. 6). 23.45° is the axial tilt of the earth.

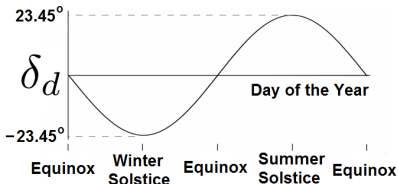


Figure 6: Declination angle δ_d throughout the year

The hour angle ω_t is defined as the angle between the meridian that intersects with the line that points to the sun and the meridian containing the observer (cf. Fig. 7(b)). The hour angle ω_t is depicted for Greenwich (London, UK) in Fig. 8. Because Greenwich (London, UK) is located on the reference meridian of its time zone, the straight line in Fig. 8 intersects the x-axis at noon². ω_t has a period of 24 hours and ranges from -180° to 180° .

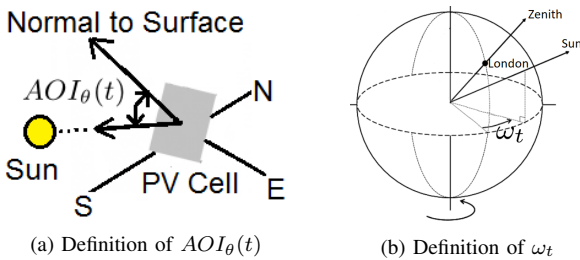


Figure 7: Depiction of the angle of incidence $AOI_\theta(t)$ and the hour angle ω_t

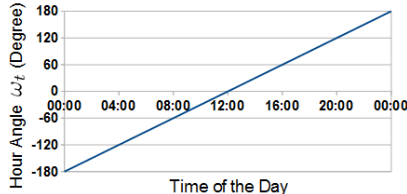


Figure 8: Hour angle ω_t throughout the day of a PV cell located on the reference meridian of its time zone

D. Sky-Diffuse Irradiance $I_{d\theta}(t)$

The sky-diffuse irradiance $I_{d\theta}(t)$ can be calculated by (12) located at the top of the next page, which is derived from the Reindl model³ [23], [24]. A_t in (12) is the anisotropy index, and ζ_t in (12) is the solar zenith angle. The Reindl model breaks the diffuse-sky irradiance into three separate parts: the isotropic component, the circumsolar component, and the

²The hour angles ω_t of locations that are not on their reference meridian of their time zone can be depicted by a straight line as well which is shifted along the x-axis. The formula to calculate the x-axis shift is given in [22].

³The difference between different irradiance models are usually in the way they model the sky-diffuse irradiance. The simplest and most commonly used model is the Liu and Jordan model, which assumes an isotropic diffuse sky [8]. In other words, the diffuse-sky irradiance is uniform across the sky and hence, the diffuse-sky irradiance is independent of the orientation angle θ . We use the more advanced Reindl model, which breaks the diffuse-sky irradiance into three separate parts: the isotropic component, the circumsolar component, and the horizon brightening component. The first component is the same as the Liu and Jordan model, while the other components are small correction terms, which are dependent on the orientation angle θ .

horizon brightening component (cf. (12)). The circumsolar component and the horizon brightening component depend on the orientation angle θ .

The solar zenith angle ζ_t can be calculated by [25] as follows:

$$\cos(\zeta_t) = \sin(lat) \sin(\delta_d) + \cos(lat) \cos(\delta_d) \cos(\omega_t) \quad (13)$$

The anisotropy index A_t can be calculated by [23] as follows:

$$A_t = \frac{DNI_t}{E_d}, \quad (14)$$

where E_d is the extraterrestrial radiation. It can be calculated by [26] as follows:

$$E_d = E_{\text{con}} \cdot \left(\frac{\bar{r}}{r_d} \right)^2 = E_{\text{con}} \cdot \left(1 + 0.033 \cos \left(\frac{360 \cdot d}{365} \right) \right), \quad (15)$$

where E_{con} is the solar constant $1367 \frac{\text{W}}{\text{m}^2}$ [20], \bar{r} is the mean sun-earth distance also called 1 astronomical unit (1 AU), r_d is the actual sun-earth distance, which depends on the day of the year, and d is the day of the year with 1st of January as $d = 1$.

E. Energy Consumption

The energy consumption of the BS at time step t is denoted by $C(t)$, which consists of a load-dependent part and a load-independent part. We investigate three different load scenarios: a BS deployed with constant traffic load $C_{\text{con}}(t)$, with business-area traffic load $C_{\text{bus}}(t)$, and with residential-area traffic load $C_{\text{res}}(t)$ (cf. Fig. 9). It can be observed that the traffic load in a business area is significantly higher during business hours than the rest of the day, while it drops a bit during lunch hours. The traffic load in a residential area is anti-correlated to the traffic load in a business area because it is higher during times when people are usually not working with its peak during late evening.

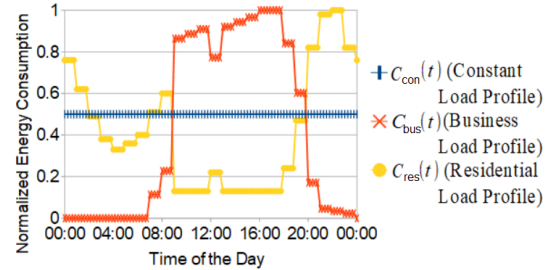
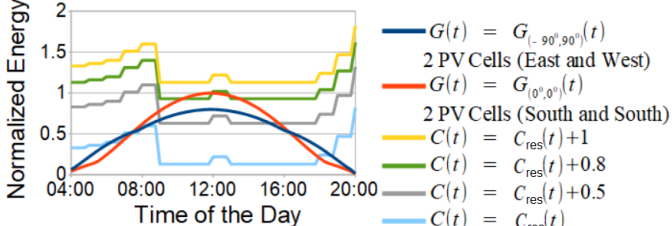
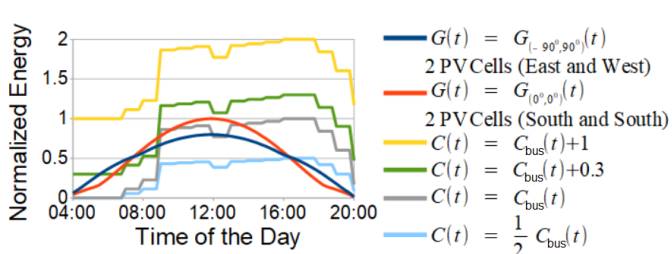
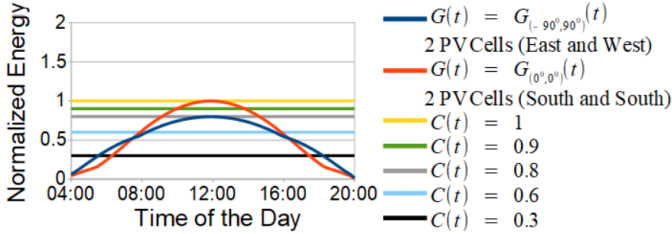


Figure 9: Constant traffic load profile, business traffic load profile, and residential traffic load profile throughout the day
Data source: [27]

Figs. 10-12 show all energy consumption profiles $C(t)$ which we will investigate. To see the relationships between the energy consumption profiles $C(t)$ and the energy generation profiles $G(t)$, the combined energy generation profile of two south-oriented PV cells $G_{(0^\circ, 0^\circ)}(t)$ as well as the combined energy generation profile of an east-oriented PV cell with a west-oriented PV cell $G_{(-90^\circ, 90^\circ)}(t)$ are shown.

$$\begin{aligned}
I_{d_\theta}(t) = & DHI_t \left[A_t \cdot \frac{\max(0, \cos(AOI_\theta(t)))}{\cos(\zeta_t)} + (1 - A_t) \cdot \frac{1 + \cos(\gamma)}{2} \cdot \left(1 + \sqrt{\frac{DNI_t \cdot \cos(\zeta_t)}{GHI_t}} \sin^3\left(\frac{\gamma}{2}\right) \right) \right] = \\
& \underbrace{DHI_t \cdot A_t \cdot \frac{\max(0, \cos(AOI_\theta(t)))}{\cos(\zeta_t)}}_{\text{Circumsolar Component}} + \underbrace{DHI_t \cdot (1 - A_t) \cdot \frac{1 + \cos(\gamma)}{2}}_{\text{Isotropic Component}} + \\
& \underbrace{DHI_t \cdot (1 - A_t) \cdot \frac{1 + \cos(\gamma)}{2} \cdot \sqrt{\frac{DNI_t \cdot \cos(\zeta_t)}{GHI_t}} \sin^3\left(\frac{\gamma}{2}\right)}_{\text{Horizon Brightening Component}}
\end{aligned} \tag{12}$$



F. Problem Formulation

The optimization objective is to minimize the energy drawn from the main grid $f(\theta_1, \dots, \theta_N)$ by the BS throughout the day which is defined in (16). The optimization problem is formulated as follows:

$$f(\theta_1, \dots, \theta_N) = \sum_{t=1}^T \max\{0, C(t) - G_{(\theta_1, \dots, \theta_N)}(t)\} \tag{16}$$

$$(\theta_1^*, \dots, \theta_N^*) = \arg \min_{(\theta_1, \dots, \theta_N)} f(\theta_1, \dots, \theta_N), \tag{17}$$

where $(\theta_1^*, \dots, \theta_N^*)$ are the optimized orientation angles for the N PV cells.

Because surplus energy is wasted in our system model, we have to take the maximum out of 0 and $C(t) - G_{(\theta_1, \dots, \theta_N)}(t)$ in (16). We simplify $f(\theta_1, \dots, \theta_N)$ in (18)-(20).

$$f(\theta_1, \dots, \theta_N) = \sum_{t=1}^T \max \left\{ 0, C(t) - \sum_{n=1}^N G_{\theta_n, N}(t) \right\} \tag{18}$$

$$= \sum_{t=1}^T \max \left\{ 0, C(t) - \underbrace{\frac{I_g(t)}{614 \frac{W}{m^2}}}_{I_{fix}(t)} - \sum_{n=1}^N \frac{I_{b_{\theta_n}}(t) + I_{d_{\theta_n}}(t)}{614 \frac{W}{m^2} \cdot N} \right\} \tag{19}$$

$$= \sum_{t=1}^T \max \left\{ 0, I_{fix}(t) - \sum_{n=1}^N \frac{I_{b_{\theta_n}}(t) + I_{d_{\theta_n}}(t)}{614 \frac{W}{m^2} \cdot N} \right\} \tag{20}$$

The gain Δ_n of adding the n^{th} PV cell with optimized orientation angle θ_n^* to the system model is defined as follows:

$$\Delta_n = f(\theta_1^*, \dots, \theta_{n-1}^*) - f(\theta_1^*, \dots, \theta_n^*) \quad n \in \{2, \dots, N\} \tag{21}$$

The gain of adding the first PV cell with optimized orientation angle θ_1^* to the system model is defined as follows:

$$\Delta_1 = f(0^\circ) - f(\theta_1^*) \tag{22}$$

A positive (negative) Δ_n value represents an improvement (deterioration) in performance of the system if the n^{th} PV cell is added, $n \in \{1, \dots, N\}$.

III. ANALYTICAL CONSIDERATIONS

This section identifies and discusses analytically to what extent the orientation angle θ shifts the energy generation profile away from noon if the PV cells are not south-oriented ($\theta \neq 0^\circ$). The direct-beam irradiance $I_{b_\theta}(t)$ and the sky-diffuse irradiance $I_{d_\theta}(t)$ depend on θ . Nonetheless, because the main component of the sky-diffuse irradiance is independent of θ (isotropic component), while the other two components, which are dependent on θ , are small correction terms, we will focus on the direct-beam irradiance in this section.

Fig. 13 shows the values of a_t , b_t , and c_t throughout one day for the spring equinox ($d = 81$), summer solstice ($d = 172$), autumn equinox ($d = 264$), and winter solstice ($d = 355$). We fix γ to 36° , and the location to Greenwich ($lat = 51.4767^\circ$ North, $lon = 0.0003^\circ$ West) to calculate the a_t , b_t , and c_t

values. Only the hour angle ω_t changes throughout the day, whereas all other parameters are constant throughout the day in (8) - (10). Therefore, a_t , b_t , and c_t have a sine or cosine behavior with the y-axis shifts and amplitudes are summarized in (23) - (25). Because ω_t has a period of 24 hours, a_t , b_t , and c_t have a period of 24 hours as well. The only angle that changes for different seasons is δ_d because it depends on the day of the year d . Therefore, the differences between the four a_t curves, the four b_t curves as well as the four c_t curves are caused only by δ_d . The curves for the spring equinox and autumn equinox are identical, i.e., $a_t(d=81)=a_t(d=264)$, $b_t(d=81)=b_t(d=264)$, and $c_t(d=81)=c_t(d=264)$.

$$a_t = \underbrace{+ \sin(\delta_d) \sin(lat) \cos(\gamma)}_{\text{y-axis shift}} + \underbrace{\cos(\delta_d) \cos(lat) \cos(\gamma) \cos(\omega_t)}_{\text{amplitude}} \quad (23)$$

$$b_t = \underbrace{+ \cos(\delta_d) \sin(\gamma) \sin(\omega_t)}_{\text{amplitude}} \quad (24)$$

$$c_t = \underbrace{- \sin(\delta_d) \cos(lat) \sin(\gamma)}_{\text{y-axis shift}} + \underbrace{\cos(\delta_d) \sin(lat) \sin(\gamma) \cos(\omega_t)}_{\text{amplitude}} \quad (25)$$

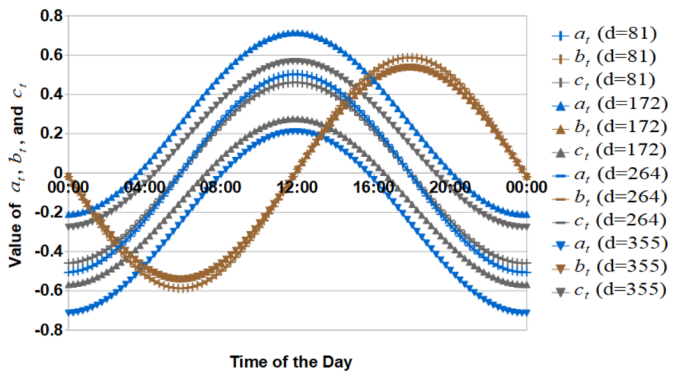


Figure 13: Values of a_t , b_t , and c_t throughout one day for the spring equinox ($d = 81$), summer solstice ($d = 172$), autumn equinox ($d = 264$), and winter solstice ($d = 355$). γ is set at 36° , and the location is Greenwich ($lat = 51.4767^\circ$ North, $lon = 0.0003^\circ$ West) for all scenarios.

We obtain the following insights from (23) to (25):

- a_t and c_t are symmetrical to noon. Hence, if $\theta \neq 0^\circ$, i.e., $\sin(\theta) \neq 0$, b_t is solely responsible for shifting the energy generation peak towards the morning or afternoon hours. If θ is orientated eastwards (westwards), then $\theta < 0$ ($\theta > 0$), and $\sin(\theta) < 0$ ($\sin(\theta) > 0$), and hence the energy generation peak is shifted toward the morning (afternoon) hours.
- Also (6) causes an asymmetric energy generation profile if $\theta \neq 0^\circ$. The max in (6) removes the direct-beam irradiance if the PV cell is illuminated from the back. The more the PV cell is orientated eastwards (westwards), the longer the PV cell is illuminated from the back in

the evening (morning) and the more energy is lost in the evening (morning).

- If the location of the PV cell is at the equator, the PV cell should be installed with the default inclination angle $\gamma = 0^\circ$ (cf. Table I). As a consequence, $\sin(\gamma) = 0$, and $b_t = c_t = 0$. As a result, any orientation angle can be chosen for a PV cell at the equator because the orientation angle does not affect the energy generation profile of a PV cell at the equator. Hence, orientation angle optimization should be done for PV cells a bit farther away from the equator, where PV cells are not horizontally mounted. Alternatively, PV cells at the equator can be inclined ($\gamma \neq 0^\circ$) a bit to facilitate orientation angle optimization at the cost of reducing the average daily energy yield of the PV cells.
- The amplitude of b_t is equal to the amplitude of c_t at the north and south poles, whereas the amplitude of b_t is greater than the amplitude of c_t at any other location.

IV. RESULTS AND DISCUSSION

Table II summarizes all parameters and their values.

A. Remarks on the Presentation of the Results

We will investigate the optimal orientation angle(s) for 1, 2, and 3 PV cell(s) in subsections IV-A1, IV-A2, and IV-A3, respectively. We will find the optimal orientation angle for each PV cell in the whole range from -90° to 90° with an angular resolution of 1° . We will optimize the orientation angle(s) in each subsection for three different types of load profiles: the constant load profile $C_{\text{con}}(t)$, the business load profile $C_{\text{bus}}(t)$, and the residential load profile $C_{\text{res}}(t)$ (cf. Fig. 9). The left, middle, and right columns in the Tables III - V represent the constant, business, and residential load profiles, respectively. Each row in the Tables III - V represents the relative relationship between the energy generation profile and energy consumption profile. In other words, the first, second, third, and fourth rows in the Tables III - V represent the scenario that the energy generation is significantly smaller, is slightly smaller, is slightly greater, is significantly greater than the energy consumption, denoted by $G \ll C$, $G < C$, $G > C$, and $G \gg C$, respectively. The red points in the Tables IV - V as well as the red lines in Table III are the optimal orientation angles. Each square in Table IV has one line of symmetry $L := \{(\theta_1, \theta_2) \in [-90^\circ, 90^\circ]^2 \mid \theta_1 = \theta_2\}$. Each cube in Table V has three planes of symmetry: $P_1 := \{(\theta_1, \theta_2, \theta_3) \in [-90^\circ, 90^\circ]^3 \mid \theta_2 = \theta_3\}$, $P_2 := \{(\theta_1, \theta_2, \theta_3) \in [-90^\circ, 90^\circ]^3 \mid \theta_1 = \theta_3\}$, and $P_3 := \{(\theta_1, \theta_2, \theta_3) \in [-90^\circ, 90^\circ]^3 \mid \theta_1 = \theta_2\}$. The graphs in the Tables III - V are generated with MATLAB.

To evaluate the effects of different numbers of PV cells, we use the same consumption profile $C(t)$ among corresponding table cells in different tables whenever possible. For example, the table cell (a) of Table III corresponds to the table cell (a) of Table IV and to the table cell (a) of Table V. The comparisons between the different tables are fair because the total surface area A is constant. In other words, we will not add more

surface area by adding another PV cell, instead we divide the total surface area A among N PV cells in each scenario. The only exception is that the table cells (d), (g), and (j) of Table III cannot be compared directly to Table IV or Table V because their energy consumption profile $C(t)$ is different.

Table II:
SUMMARY OF ALL PARAMETERS

| Parameter | Description | Value |
|--------------------------------------|---|---|
| α | Albedo | 0.2 (Grassland) |
| γ | Inclination angle | 36° |
| δ_d | Declination angle | Eq. (11) |
| ζ_t | Zenith angle | Eq. (13) |
| θ | Orientation angle | $\in [-90^\circ, 90^\circ]$ |
| $\theta_1, \dots, \theta_N$ | Orientation angles of PV cells 1, ..., N | $\in [-90^\circ, 90^\circ]$ |
| $\theta_1^*, \dots, \theta_N^*$ | Optimized orientation angles $\theta_1^*, \dots, \theta_N^*$ | $\in [-90^\circ, 90^\circ]$ |
| ω_t | Hour angle | Fig. 8 |
| Δ_1 | Gain of adding the 1 st PV cell | Eq. (22) |
| Δ_n | Gain of adding the n^{th} PV cell, $n \in \{2, \dots, N\}$ | Eq. (21) |
| A | Total surface area of N PV cells | 1m ² |
| A_t | Anisotropy index | Eq. (14) |
| $AOI_\theta(t)$ | Angle of incidence | Eq. (7) |
| $C(t)$ | Energy consumption of BS | Figs. 10 - 12 |
| $C_{\text{bus}}(t)$ | Business-area traffic load profile | Fig. 9 |
| $C_{\text{con}}(t)$ | Constant traffic load profile | Fig. 9 |
| $C_{\text{res}}(t)$ | Residential-area traffic load profile | Fig. 9 |
| DHI_t | Diffuse horizontal irradiance | PVGIS [17] |
| DNI_t | Direct normal irradiance | PVGIS [17] |
| E_d | Extraterrestrial radiation | Eq. (15) |
| E_{con} | Solar constant | 1367 $\frac{\text{W}}{\text{m}^2}$ [20] |
| $G(t)$ | Energy generation of PV cell/cells | |
| $G_{\theta, N}^{\text{original}}(t)$ | Energy generated by one PV cell installed with θ (N is the total number of PV cells) | Eq. (1) |
| $G_{\theta, N}(t)$ | Normalized energy generated by one PV cell installed with θ (N is the total number of PV cells) | Eq. (2) |
| $G_{(\theta_1, \dots, \theta_N)}(t)$ | Normalized total energy generated by N PV cells installed with $\theta_1, \dots, \theta_N$ | Eq. (3) |
| GHI_t | Global horizontal irradiance | PVGIS [17] |
| $I_\theta(t)$ | Irradiance on PV cell installed with θ | |
| $I_{b_\theta}(t)$ | Direct-beam irradiance | Eq. (4) |
| $I_{d_\theta}(t)$ | Sky-diffuse irradiance | Eq. (6) |
| $I_g(t)$ | Ground-reflected irradiance | Eq. (12) |
| N | Number of PV cells | Eq. (5) |
| T | Number of time steps | $\in \{1, 2, 3\}$ |
| a_t | Independent of θ | 96 |
| b_t | Multiplied by $\sin(\theta)$ | Eq. (8) |
| c_t | Multiplied by $\cos(\theta)$ | Eq. (9) |
| d | Day of the year | Eq. (10) |
| $f(\theta_1, \dots, \theta_N)$ | Optimization objective | 165 (June) |
| lat | Latitude | Eq. (16) |
| lon | Longitude | 51.4767° North (Greenwich) |
| | | 0.0003° West (Greenwich) |

We use normalized energy generation and consumption profiles in this paper. That means the given recommendations in this section can be scaled up for the intended application in the real world. For example, if the derived recommendation

for the normalized consumption profile $C(t)$ is to deploy one PV cell with optimized orientation angel θ_1^* , that means to deploy several PV cells with the same orientation angle θ_1^* in the real world if $C(t)$ was the consumption profile of a large-scale BS. Another example, if the derived recommendation for the normalized consumption profile $C(t)$ is to deploy two PV cells with jointly optimized orientation angles θ_1^* and θ_2^* , that means to deploy several PV cells where half of them are deployed with θ_1^* and the other half with θ_2^* in the real world if $C(t)$ was the consumption profile of a large-scale BS.

1) 1 PV cell ($N=1$) : Table III and Table VI show the results for 1 PV cell.

2) 2 PV cells ($N=2$) : Table IV and Table VII show the results for 2 PV cells.

3) 3 PV cells ($N=3$) : Table V and Table VIII show the results for 3 PV cells. The y-axis (θ_2 -axis) is reversed in all business load profile scenarios (second column of Table V) so that the optimal points are visible.

B. Summary of the Key Findings

If $G \ll C$ (first rows in Tables VI - VIII), all PV cells should be oriented towards the south, i.e., the optimal orientation angles are $\theta_1^* = \theta_2^* = \dots = \theta_N^* = 0^\circ$. If $G \gg C$, the optimal orientation angles are independent of the shape of the energy consumption profile.

The optimal orientation angles change from south orientation in the $G \ll C$ scenarios towards the east and/or west orientation in the $G \gg C$ scenarios in every column of the Tables III - V. The optimal orientation angles in the $G < C$ scenarios are closer to the south orientation than the east and/or west orientation, whereas the optimal orientation angles in the $G > C$ scenarios are closer to the east and/or west orientation than the south orientation.

We will evaluate the gains of adding the first, second, and third PV cell with optimized orientation angle to the system model in the following paragraphs.

1) *PV cells with default orientation angles*: The centers of the stripes, squares, and cubes in Table III, Table IV, and Table V are the normalized energy drawn from the main grid, i.e, $f(0^\circ)$, $f(0^\circ, 0^\circ)$, and $f(0^\circ, 0^\circ, 0^\circ)$, if no orientation angle optimization is performed, respectively. PV cells are oriented towards the south in the northern hemisphere by default (cf. Table I). $f(0^\circ) = f(0^\circ, 0^\circ) = f(0^\circ, \dots, 0^\circ)$ if the same consumption profile $C(t)$ is used because the total surface area A in the system model is constant. For example, $f(0^\circ)$ in Table III(a) equals to $f(0^\circ, 0^\circ)$ in Table IV(a) and $f(0^\circ, 0^\circ, 0^\circ)$ in Table V(a).

2) *Adding the first PV cell with optimized orientation angle*: A positive (negative) Δ_1 value represents an improvement (deterioration) in performance of the system if the first PV cell is added. $\Delta_1 > 0$ for the table cells (d)-(l) and $\Delta_1 = 0$ for the table cells (a)-(c) in Table VI. The greatest Δ_1 values for the constant, business, and residential load profiles in Table VI are 0.3829 (table cell (j)), 2.3318 (table cell (h)), and 1.5493 (table cell (l)), respectively. The optimized values $f(\theta_1^*)$ (red lines in Table III) are usually significantly greater than the

default values $f(0^\circ)$ (centers of the stripes in Table III). In other words, orientation angle optimization improves the system performance in most scenarios. Δ_1 is always greater or equal to 0 because $f(0^\circ) \geq f(\theta_1^*)$. That means the system performance can only be improved and will never worsen by adding the first PV cell. We want to point out that a load profile type can have an optimal orientation angle on the east side ($\theta^* < 0$), on the west side ($\theta^* > 0$), as well as oriented southwards ($\theta^* = 0$) in different scenarios as it can be seen for the residential load profiles (third column) in Table III.

3) Adding the second PV cell with optimized orientation angle: $\Delta_2 > 0$ for all table cells in Table VII with two optimal points, i.e., (d), (f)-(g), and (i)-(j). $\Delta_2 = 0$ for all table cells in Table VII with only one optimal point, i.e., (a)-(c), (e), (h), and (k)-(l). The greatest Δ_2 values for the constant, business, and residential load profiles in Table VII are 2.0891 (table cell (j)), 0 (table cells (b), (e), (h), and (k)), and 0.5424 (table cell (i)), respectively. The Δ_2 values are usually smaller than the Δ_1 values for the business and residential load profiles, whereas the Δ_2 values are usually greater than the Δ_1 values for the constant load profiles. Consumption profiles which are similar to the constant profile, e.g., the scenarios in the first column, can often improve their performance ($\Delta_2 > 0$) by choosing orientation angles with opposite algebraic signs, e.g., $\theta_1^* > 0^\circ$ and $\theta_2^* < 0^\circ$, as seen in table cells (d), (g), and (j) in Table VII. Consumption profiles which have significant local maxima in the morning as well as in the afternoon, e.g., the residential load profile scenarios in the third column, can often improve their performance ($\Delta_2 > 0$) by choosing orientation angles with opposite algebraic signs, e.g., $\theta_1^* > 0^\circ$ and $\theta_2^* < 0^\circ$, as seen in table cells (f), and (i) in Table VII. Consumption profiles which have only one significant maximum, e.g., the business load profile scenarios in the second column, cannot improve their performance ($\Delta_2 = 0$) by adding a second PV cell.

4) Adding the third PV cell with optimized orientation angle: $\Delta_3 > 0$ for the table cell (l) in Table VIII. $\Delta_3 = 0$ for all table cells in Table VIII with only one optimal point, i.e., (a)-(c), (e), (h), and (k). $\Delta_3 < 0$ for the table cells (d), (f)-(g), and (i)-(j) in Table VIII. The greatest and lowest Δ_3 values for the constant, business, and residential load profiles in Table VIII are 0 and -0.3361 , 0 and 0, and 0.1494 and -0.0296 , respectively. The Δ_3 values are usually smaller than the Δ_2 values and sometimes even negative. That means that adding the third PV cell only improves the system performance slightly in some rare scenarios, whereas the system performance worsens in most other scenarios. Consumption profiles which are similar to the constant profile worsen their performance ($\Delta_3 < 0$) in most scenarios because 3 PV cells cannot equally shift the energy generation peak towards the morning and afternoon hours. Either two PV cells have positive algebraic signs and one PV cell has a negative algebraic sign or the other way around as seen in table cells (d), (g), and (j) in Table VIII. Consumption profiles which have two significant local maxima in the morning as well as in the afternoon, e.g., the residential load profile scenarios in the third column, can slightly improve

($\Delta_3 > 0$) or slightly worsen ($\Delta_3 < 0$) their performance as seen in table cells (l), and (i) in Table VIII. Consumption profiles which have only one significant maximum, e.g., the business load profile scenarios in the second column, cannot improve their performance ($\Delta_3 = 0$) by adding a third PV cell. In general, consumption profiles which have three significant local maxima between sunrise and sunset might benefit in some scenarios from 3 PV cells. But it becomes harder and harder to find such specific consumption profiles and scenarios to justify that 3 or more PV cells are necessary to improve the system performance significantly.

V. CONCLUSION

We have shown that the system performance ($\Delta_1 > 0$) can be increased significantly by deploying one PV cell with optimized orientation angle θ_1^* (or several PV cells with the same orientation angle θ_1^*) if the energy generation is slightly smaller ($G < C$), is slightly greater ($G > C$), or is significantly greater ($G \gg C$) than the energy consumption. This is caused by the ability to shift the energy generation peak from noon towards the most significant local maximum between sunrise and sunset of the energy consumption profile. Furthermore, the system performance ($\Delta_2 > 0$) can be further increased by deploying two PV cells with jointly optimized orientation angles θ_1^* and θ_2^* (or several PV cells where half of them are deployed with θ_1^* and the other half with θ_2^*) if a constant energy consumption profile or a consumption profile with significant local maxima in the morning as well as in the afternoon is given. This is caused by the ability to shift the energy generation peak from noon towards the morning with east-oriented PV cells, while the other west-oriented PV cells shift the energy generation peak towards the afternoon in the northern hemisphere. Because there are only two directions (morning and afternoon) that the energy can be shifted to, more than two PV cells usually does not further increase the performance significantly. More than 2 differently oriented PV cells may even degrade the system performance ($\Delta_3 < 0$) in some scenarios.

From a practical point of view, the optimization algorithm is faster for only a few PV cells (1 or 2 PV cells) than for several PV cells (more than 2 PV cells). In addition, if there are several PV cells with different optimal orientation angles, the spacing between the differently oriented PV cells has to be sufficient enough to avoid shadowing effects on the panels. This increases the area needed for deployment of the PV cells. Furthermore, it is not possible to mount PV cells with different orientation angles on the same array or support structure which increases the material cost for buying several arrays or support structures. Hence, we recommend to do orientation angle optimization with one PV cell for energy consumption profiles which have one significant local maximum between sunrise and sunset and with two PV cells for energy consumption profiles which have significant local maxima in the morning as well as in the afternoon or constant energy consumption profiles.

REFERENCES

- [1] G. Piro, M. Miozzo, G. Forte, N. Baldo, L. A. Grieco, G. Boggia, and P. Dini, "HetNets powered by renewable energy sources: Sustainable next-generation cellular networks," *IEEE Internet Computing*, vol. 17, no. 1, pp. 32–39, Jan 2013.
- [2] Y. Mao, Y. Luo, J. Zhang, and K. B. Letaief, "Energy harvesting small cell networks: feasibility, deployment, and operation," *IEEE Communications Magazine*, vol. 53, no. 6, pp. 94–101, Jun 2015.
- [3] A. Kwasinski and A. Kwasinski, "Increasing sustainability and resiliency of cellular network infrastructure by harvesting renewable energy," *IEEE Communications Magazine*, vol. 53, no. 4, pp. 110–116, Apr 2015.
- [4] R. Luthander, J. Widén, D. Nilsson, and J. Palm, "Photovoltaic self-consumption in buildings: A review," *Applied Energy*, vol. 142, pp. 80 – 94, 2015.
- [5] A. Luque and S. Hegedus, *Handbook of Photovoltaic Science and Engineering*, 2nd ed. Chichester, United Kingdom: John Wiley & Sons, Ltd, 2011, pp. 8–9.
- [6] J. Ordóñez, E. Jadraque, J. Alegre, and G. Martínez, "Analysis of the photovoltaic solar energy capacity of residential rooftops in Andalusia (Spain)," *Renewable and Sustainable Energy Reviews*, vol. 14, no. 7, pp. 2122 – 2130, 2010.
- [7] L. G. Valladares-Rendón, G. Schmid, and S.-L. Lo, "Review on energy savings by solar control techniques and optimal building orientation for the strategic placement of façade shading systems," *Energy and Buildings*, vol. 140, pp. 458 – 479, 2017.
- [8] Y. S. Khoo, A. Nobre, R. Malhotra, D. Yang, R. Ruther, T. Reindl, and A. G. Aberle, "Optimal orientation and tilt angle for maximizing in-plane solar irradiation for PV applications in Singapore," *IEEE Journal of Photovoltaics*, vol. 4, no. 2, pp. 647–653, 2014.
- [9] B. P. Kemery, I. Beausoleil-Morrison, and I. H. Rowlands, "Optimal PV orientation and geographic dispersion: a study of 10 Canadian cities and 16 Ontario locations," in *The Canadian Conference on Building Simulation*, 2012.
- [10] D. Benda, X. Chu, S. Sun, T. Q. S. Quek, and A. Buckley, "Renewable energy sharing among base stations as a min-cost-max-flow optimization problem," *IEEE Transactions on Green Communications and Networking*, vol. 3, no. 1, pp. 67–78, March 2019.
- [11] D. Benda, X. Chu, S. Sun, T. Q. S. Quek, and A. Buckley, "Modeling and optimization of energy sharing among base stations as a minimum-cost-maximum-flow problem," in *Proc. IEEE VTC-Spring*, Porto, Portugal, Jun 2018.
- [12] K. Chattopadhyay, A. Kies, E. Lorenz, L. von Bremen, and D. Heinemann, "The impact of different PV module configurations on storage and additional balancing needs for a fully renewable European power system," *Renewable Energy*, vol. 113, pp. 176 – 189, 2017.
- [13] A. H. Khan, K. R. Zafreen, A. Islam, and M. Islam, "Shifting generation of energy of solar PV using OPTANG method-case study Sandwip area," in *Proc. 3rd ICGET*, Dhaka, Bangladesh, Sep 2015.
- [14] D. Benda, S. Sun, X. Chu, T. Q. S. Quek, and A. Buckley, "PV cell angle optimization for energy generation-consumption matching in a solar powered cellular network," *IEEE Transactions on Green Communications and Networking*, vol. 2, no. 1, pp. 40–48, March 2018.
- [15] D. Benda, X. Chu, S. Sun, T. Q. S. Quek, and A. Buckley, "PV cell orientation angle optimization for a solar energy harvesting base station," in *Proc. IEEE GLOBECOM*, Singapore, Dec 2017.
- [16] D. Benda, X. Chu, S. Sun, T. Q. S. Quek, and A. Buckley, "PV cell angle optimisation for energy arrival-consumption matching in a solar energy harvesting cellular network," in *Proc. IEEE ICC*, Paris, France, May 2017.
- [17] European Commission. (2016) Photovoltaic geographical information system (PVGIS). [Online]. Available: <http://re.jrc.ec.europa.eu/pvgis/>
- [18] A. Luque and S. Hegedus, *Handbook of Photovoltaic Science and Engineering*, 2nd ed. Chichester, United Kingdom: John Wiley & Sons, Ltd, 2011, p. 1002.
- [19] A. Luque and S. Hegedus, *Handbook of Photovoltaic Science and Engineering*, 2nd ed. Chichester, United Kingdom: John Wiley & Sons, Ltd, 2011, p. 1005.
- [20] A. Luque and S. Hegedus, *Handbook of Photovoltaic Science and Engineering*, 2nd ed. Chichester, United Kingdom: John Wiley & Sons, Ltd, 2011, p. 991.
- [21] A. Luque and S. Hegedus, *Handbook of Photovoltaic Science and Engineering*, 2nd ed. Chichester, United Kingdom: John Wiley & Sons, Ltd, 2011, p. 986.
- [22] A. Luque and S. Hegedus, *Handbook of Photovoltaic Science and Engineering*, 2nd ed. Chichester, United Kingdom: John Wiley & Sons, Ltd, 2011, p. 989.
- [23] P. G. Loutzenhiser, H. Manz, C. Felsmann, P. A. Strachan, T. Frank, and G. M. Maxwell, "Empirical validation of models to compute solar irradiance on inclined surfaces for building energy simulation," *Solar Energy*, vol. 81, no. 2, pp. 254–267, 2007.
- [24] A. Luque and S. Hegedus, *Handbook of Photovoltaic Science and Engineering*, 2nd ed. Chichester, United Kingdom: John Wiley & Sons, Ltd, 2011, p. 1004.
- [25] A. Luque and S. Hegedus, *Handbook of Photovoltaic Science and Engineering*, 2nd ed. Chichester, United Kingdom: John Wiley & Sons, Ltd, 2011, p. 988.
- [26] E. Akarslan, F. O. Hocaoğlu, and R. Edizkan, "A novel M-D (multi-dimensional) linear prediction filter approach for hourly solar radiation forecasting," *Energy*, vol. 73, pp. 978 – 986, 2014.
- [27] CelPlan. (2014) White paper - customer experience optimization in wireless networks. [Online]. Available: <http://www.celplan.com/resources/whitepapers/Customer%20Experience%20Optimization%20rev3.pdf>

Table III:
ORIENTATION ANGLES OPTIMIZATION FOR 1 PV CELL WITH DIFFERENT LOAD PROFILES

| | Constant Load Profile | Business Load Profile | Residential Load Profile | | | | | | | | | | | | | | | | | | | | | | | | | | | | | | |
|-----------|---|-----------------------|--------------------------|-------|----|----|------|------|------|------|------|--|-----|-----|---|----|----|-------|-----|-------|-----|-------|--|-----|-----|---|----|----|-------|------|-------|------|-------|
| $G \ll C$ | <p>Table cell (a):</p> <p>Orientation Angle of PV Cell 1 (θ_1)</p> <table border="1"> <tr><td>-90</td><td>-45</td><td>0</td><td>45</td><td>90</td></tr> <tr><td>60.5</td><td>61</td><td>61.5</td><td>62</td><td></td></tr> </table> <p>Normalized Energy drawn from the Grid</p> <p>$C(t) = 1$ (Fig. 10 yellow line)</p> | -90 | -45 | 0 | 45 | 90 | 60.5 | 61 | 61.5 | 62 | | <p>Table cell (b):</p> <p>Orientation Angle of PV Cell 1 (θ_1)</p> <table border="1"> <tr><td>-90</td><td>-45</td><td>0</td><td>45</td><td>90</td></tr> <tr><td>101.5</td><td>102</td><td>102.5</td><td>103</td><td>103.5</td></tr> </table> <p>Normalized Energy drawn from the Grid</p> <p>$C(t) = C_{\text{bus}}(t) + 1$ (Fig. 11 yellow line)</p> | -90 | -45 | 0 | 45 | 90 | 101.5 | 102 | 102.5 | 103 | 103.5 | <p>Table cell (c):</p> <p>Orientation Angle of PV Cell 1 (θ_1)</p> <table border="1"> <tr><td>-90</td><td>-45</td><td>0</td><td>45</td><td>90</td></tr> <tr><td>100.5</td><td>101</td><td>101.5</td><td>102</td><td>102.5</td></tr> </table> <p>Normalized Energy drawn from the Grid</p> <p>$C(t) = C_{\text{res}}(t) + 1$ (Fig. 12 yellow line)</p> | -90 | -45 | 0 | 45 | 90 | 100.5 | 101 | 101.5 | 102 | 102.5 |
| -90 | -45 | 0 | 45 | 90 | | | | | | | | | | | | | | | | | | | | | | | | | | | | | |
| 60.5 | 61 | 61.5 | 62 | | | | | | | | | | | | | | | | | | | | | | | | | | | | | | |
| -90 | -45 | 0 | 45 | 90 | | | | | | | | | | | | | | | | | | | | | | | | | | | | | |
| 101.5 | 102 | 102.5 | 103 | 103.5 | | | | | | | | | | | | | | | | | | | | | | | | | | | | | |
| -90 | -45 | 0 | 45 | 90 | | | | | | | | | | | | | | | | | | | | | | | | | | | | | |
| 100.5 | 101 | 101.5 | 102 | 102.5 | | | | | | | | | | | | | | | | | | | | | | | | | | | | | |
| $G < C$ | <p>Table cell (d):</p> <p>Orientation Angle of PV Cell 1 (θ_1)</p> <table border="1"> <tr><td>-90</td><td>-45</td><td>0</td><td>45</td><td>90</td></tr> <tr><td>43.8</td><td>44</td><td>44.2</td><td>44.4</td><td>44.6</td></tr> </table> <p>Normalized Energy drawn from the Grid</p> <p>$C(t) = 0.8$ (Fig. 10 gray line)</p> | -90 | -45 | 0 | 45 | 90 | 43.8 | 44 | 44.2 | 44.4 | 44.6 | <p>Table cell (e):</p> <p>Orientation Angle of PV Cell 1 (θ_1)</p> <table border="1"> <tr><td>-90</td><td>-45</td><td>0</td><td>45</td><td>90</td></tr> <tr><td>36</td><td>38</td><td>40</td><td></td><td></td></tr> </table> <p>Normalized Energy drawn from the Grid</p> <p>$C(t) = C_{\text{bus}}(t) + 0.3$ (Fig. 11 green line)</p> | -90 | -45 | 0 | 45 | 90 | 36 | 38 | 40 | | | <p>Table cell (f):</p> <p>Orientation Angle of PV Cell 1 (θ_1)</p> <table border="1"> <tr><td>-90</td><td>-45</td><td>0</td><td>45</td><td>90</td></tr> <tr><td>81.5</td><td>82</td><td>82.5</td><td>83</td><td></td></tr> </table> <p>Normalized Energy drawn from the Grid</p> <p>$C(t) = C_{\text{res}}(t) + 0.8$ (Fig. 12 green line)</p> | -90 | -45 | 0 | 45 | 90 | 81.5 | 82 | 82.5 | 83 | |
| -90 | -45 | 0 | 45 | 90 | | | | | | | | | | | | | | | | | | | | | | | | | | | | | |
| 43.8 | 44 | 44.2 | 44.4 | 44.6 | | | | | | | | | | | | | | | | | | | | | | | | | | | | | |
| -90 | -45 | 0 | 45 | 90 | | | | | | | | | | | | | | | | | | | | | | | | | | | | | |
| 36 | 38 | 40 | | | | | | | | | | | | | | | | | | | | | | | | | | | | | | | |
| -90 | -45 | 0 | 45 | 90 | | | | | | | | | | | | | | | | | | | | | | | | | | | | | |
| 81.5 | 82 | 82.5 | 83 | | | | | | | | | | | | | | | | | | | | | | | | | | | | | | |
| $G > C$ | <p>Table cell (g):</p> <p>Orientation Angle of PV Cell 1 (θ_1)</p> <table border="1"> <tr><td>-90</td><td>-45</td><td>0</td><td>45</td><td>90</td></tr> <tr><td>30</td><td>30.1</td><td>30.2</td><td>30.3</td><td></td></tr> </table> <p>Normalized Energy drawn from the Grid</p> <p>$C(t) = 0.6$ (Fig. 10 light blue line)</p> | -90 | -45 | 0 | 45 | 90 | 30 | 30.1 | 30.2 | 30.3 | | <p>Table cell (h):</p> <p>Orientation Angle of PV Cell 1 (θ_1)</p> <table border="1"> <tr><td>-90</td><td>-45</td><td>0</td><td>45</td><td>90</td></tr> <tr><td>12</td><td>14</td><td>16</td><td>18</td><td></td></tr> </table> <p>Normalized Energy drawn from the Grid</p> <p>$C(t) = C_{\text{bus}}(t)$ (Fig. 11 gray line)</p> | -90 | -45 | 0 | 45 | 90 | 12 | 14 | 16 | 18 | | <p>Table cell (i):</p> <p>Orientation Angle of PV Cell 1 (θ_1)</p> <table border="1"> <tr><td>-90</td><td>-45</td><td>0</td><td>45</td><td>90</td></tr> <tr><td>58</td><td>58.5</td><td>59</td><td>59.5</td><td></td></tr> </table> <p>Normalized Energy drawn from the Grid</p> <p>$C(t) = C_{\text{res}}(t) + 0.5$ (Fig. 12 gray line)</p> | -90 | -45 | 0 | 45 | 90 | 58 | 58.5 | 59 | 59.5 | |
| -90 | -45 | 0 | 45 | 90 | | | | | | | | | | | | | | | | | | | | | | | | | | | | | |
| 30 | 30.1 | 30.2 | 30.3 | | | | | | | | | | | | | | | | | | | | | | | | | | | | | | |
| -90 | -45 | 0 | 45 | 90 | | | | | | | | | | | | | | | | | | | | | | | | | | | | | |
| 12 | 14 | 16 | 18 | | | | | | | | | | | | | | | | | | | | | | | | | | | | | | |
| -90 | -45 | 0 | 45 | 90 | | | | | | | | | | | | | | | | | | | | | | | | | | | | | |
| 58 | 58.5 | 59 | 59.5 | | | | | | | | | | | | | | | | | | | | | | | | | | | | | | |
| $G >> C$ | <p>Table cell (j):</p> <p>Orientation Angle of PV Cell 1 (θ_1)</p> <table border="1"> <tr><td>-90</td><td>-45</td><td>0</td><td>45</td><td>90</td></tr> <tr><td>12.3</td><td>12.4</td><td>12.5</td><td>12.6</td><td></td></tr> </table> <p>Normalized Energy drawn from the Grid</p> <p>$C(t) = 0.3$ (Fig. 10 black line)</p> | -90 | -45 | 0 | 45 | 90 | 12.3 | 12.4 | 12.5 | 12.6 | | <p>Table cell (k):</p> <p>Orientation Angle of PV Cell 1 (θ_1)</p> <table border="1"> <tr><td>-90</td><td>-45</td><td>0</td><td>45</td><td>90</td></tr> <tr><td>2</td><td>3</td><td>4</td><td>5</td><td></td></tr> </table> <p>Normalized Energy drawn from the Grid</p> <p>$C(t) = \frac{1}{2}C_{\text{bus}}(t)$ (Fig. 11 light blue line)</p> | -90 | -45 | 0 | 45 | 90 | 2 | 3 | 4 | 5 | | <p>Table cell (l):</p> <p>Orientation Angle of PV Cell 1 (θ_1)</p> <table border="1"> <tr><td>-90</td><td>-45</td><td>0</td><td>45</td><td>90</td></tr> <tr><td>27</td><td>28</td><td>29</td><td></td><td></td></tr> </table> <p>Normalized Energy drawn from the Grid</p> <p>$C(t) = C_{\text{res}}(t)$ (Fig. 12 light blue line)</p> | -90 | -45 | 0 | 45 | 90 | 27 | 28 | 29 | | |
| -90 | -45 | 0 | 45 | 90 | | | | | | | | | | | | | | | | | | | | | | | | | | | | | |
| 12.3 | 12.4 | 12.5 | 12.6 | | | | | | | | | | | | | | | | | | | | | | | | | | | | | | |
| -90 | -45 | 0 | 45 | 90 | | | | | | | | | | | | | | | | | | | | | | | | | | | | | |
| 2 | 3 | 4 | 5 | | | | | | | | | | | | | | | | | | | | | | | | | | | | | | |
| -90 | -45 | 0 | 45 | 90 | | | | | | | | | | | | | | | | | | | | | | | | | | | | | |
| 27 | 28 | 29 | | | | | | | | | | | | | | | | | | | | | | | | | | | | | | | |

Table IV:
ORIENTATION ANGLES OPTIMIZATION FOR 2 PV CELLS WITH DIFFERENT LOAD PROFILES

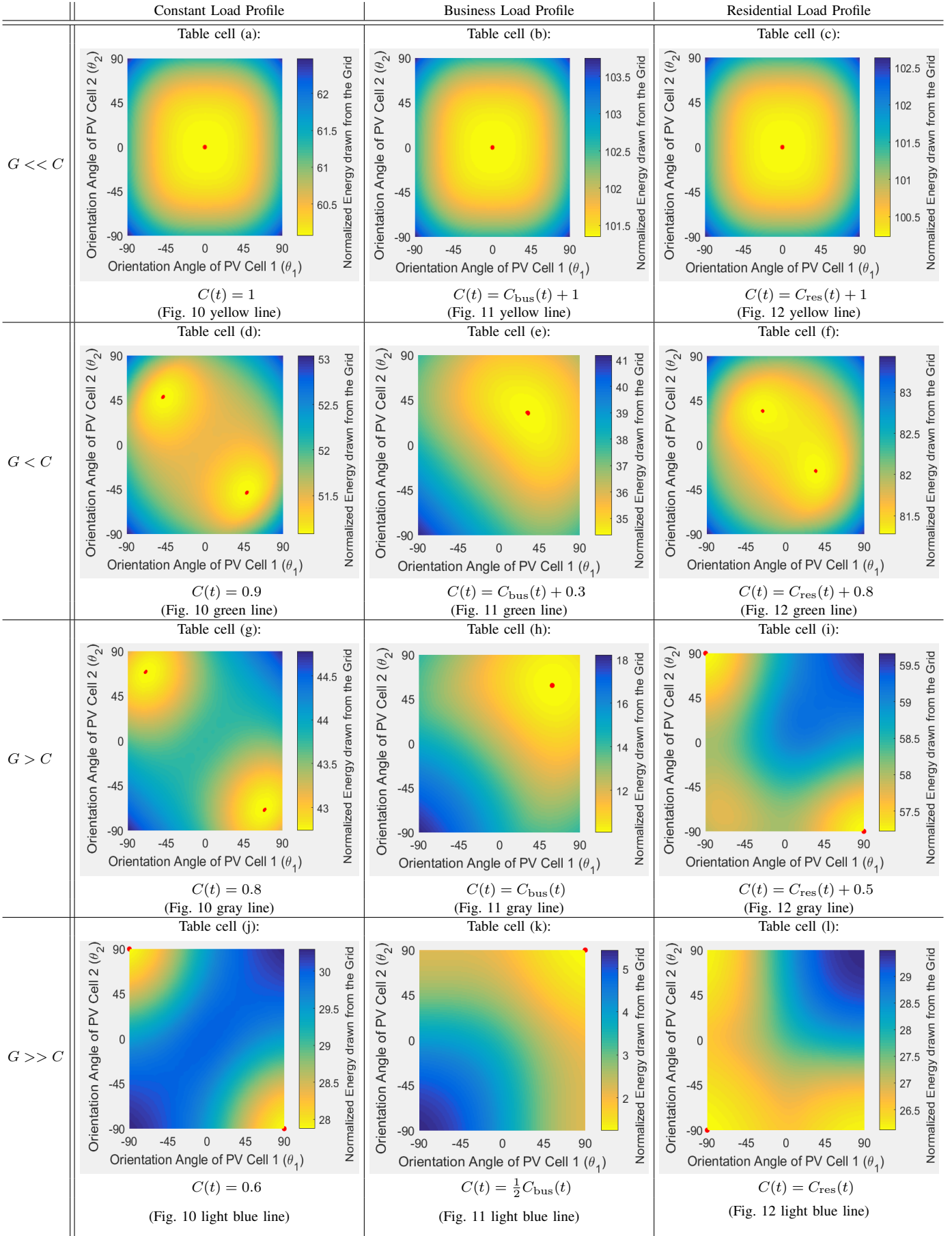


Table V:
ORIENTATION ANGLES OPTIMIZATION FOR 3 PV CELLS WITH DIFFERENT LOAD PROFILES

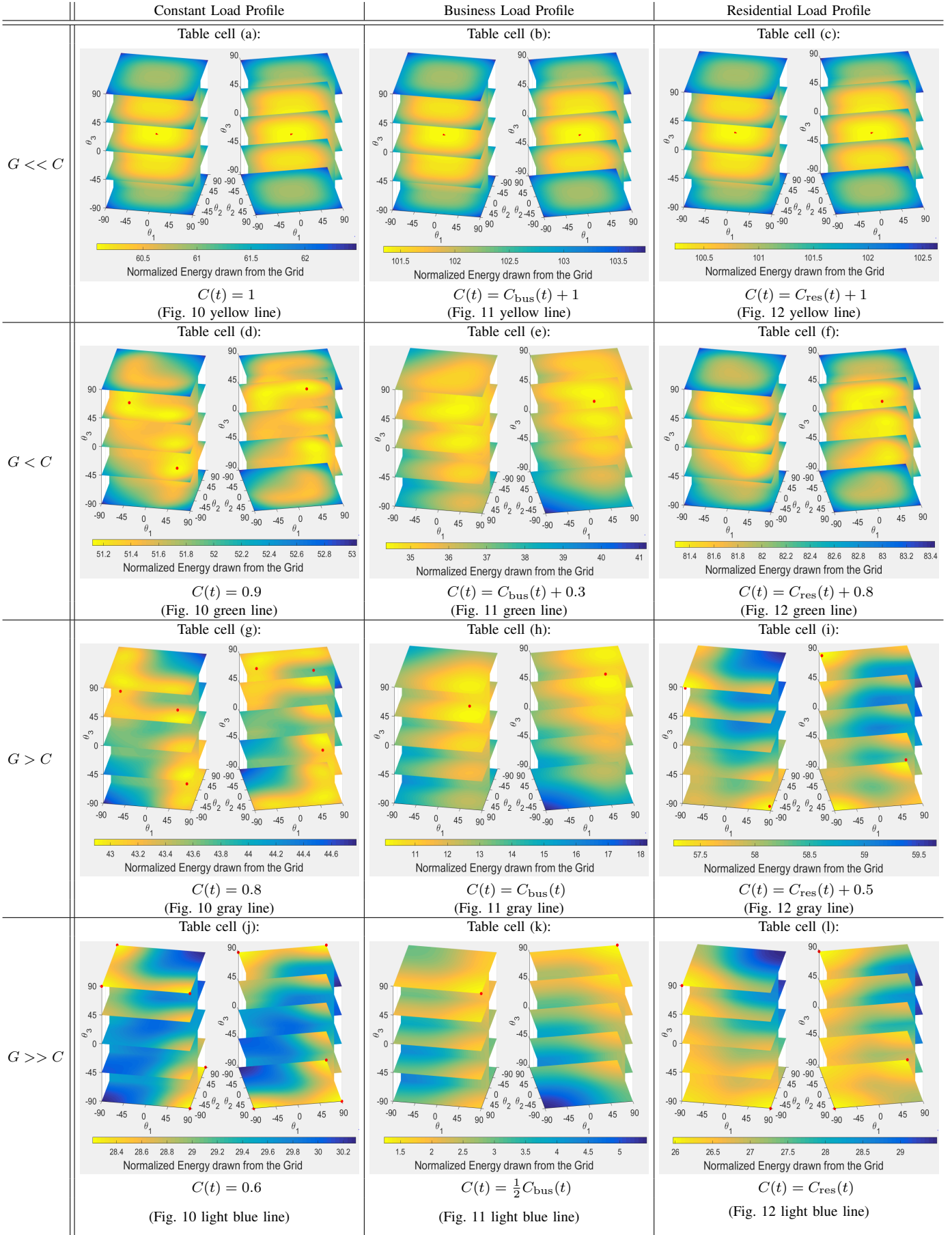


Table VI:
SUMMARY OF ALL OPTIMAL ORIENTATION ANGLES FOR 1 PV CELL WITH THE DIFFERENT LOAD PROFILES FROM TABLE III

| | | Constant Load Profile | Business Load Profile | Residential Load Profile |
|-----------|-----------------|--|--|---|
| $G \ll C$ | θ_1^* | Table cell (a) of Table III: 1 optimal line $\in \{0^\circ\}$ | Table cell (b) of Table III: 1 optimal line $\in \{0^\circ\}$ | Table cell (c) of Table III: 1 optimal line $\in \{0^\circ\}$ |
| | $f(0^\circ)$ | 60.0712 | 101.3440 | 100.2310 |
| | $f(\theta_1^*)$ | 60.0712 | 101.3440 | 100.2310 |
| | Δ_1 | 0 | 0 | 0 |
| $G < C$ | θ_1^* | Table cell (d) of Table III: 2 optimal lines $\in \{-12^\circ, 12^\circ\}$ | Table cell (e) of Table III: 1 optimal line $\in \{32^\circ\}$ | Table cell (f) of Table III: 1 optimal line $\in \{7^\circ\}$ |
| | $f(0^\circ)$ | 43.7613 | 35.2500 | 81.3698 |
| | $f(\theta_1^*)$ | 43.7530 | 34.3548 | 81.3530 |
| | Δ_1 | 0.0083 | 0.8952 | 0.0168 |
| $G \gg C$ | θ_1^* | Table cell (g) of Table III: 2 optimal lines $\in \{-35^\circ, 35^\circ\}$ | Table cell (h) of Table III: 1 optimal line $\in \{59^\circ\}$ | Table cell (i) of Table III: 1 optimal line $\in \{-70^\circ\}$ |
| | $f(0^\circ)$ | 29.9956 | 12.3939 | 59.0301 |
| | $f(\theta_1^*)$ | 29.9630 | 10.0621 | 57.7670 |
| | Δ_1 | 0.0326 | 2.3318 | 1.2631 |
| $G > C$ | θ_1^* | Table cell (j) of Table III: 2 optimal lines $\in \{-90^\circ, 90^\circ\}$ | Table cell (k) of Table III: 1 optimal line $\in \{90^\circ\}$ | Table cell (l) of Table III: 1 optimal line $\in \{-90^\circ\}$ |
| | $f(0^\circ)$ | 12.6629 | 3.3316 | 27.6658 |
| | $f(\theta_1^*)$ | 12.2800 | 1.2400 | 26.1165 |
| | Δ_1 | 0.3829 | 2.0916 | 1.5493 |

Table VII:
SUMMARY OF ALL OPTIMAL ORIENTATION ANGLES FOR 2 PV CELLS WITH THE DIFFERENT LOAD PROFILES FROM TABLE IV

| | | Constant Load Profile | Business Load Profile | Residential Load Profile |
|-----------|-----------------------------|---|--|---|
| $G \ll C$ | (θ_1^*, θ_2^*) | Table cell (a) of Table IV: 1 optimal point $\in \{(0^\circ, 0^\circ)\}$ | Table cell (b) of Table IV: 1 optimal point $\in \{(0^\circ, 0^\circ)\}$ | Table cell (c) of Table IV: 1 optimal point $\in \{(0^\circ, 0^\circ)\}$ |
| | $f(\theta_1^*, \theta_2^*)$ | 60.0712 | 101.3440 | 100.2310 |
| | Δ_2 | 0 | 0 | 0 |
| $G < C$ | (θ_1^*, θ_2^*) | Table cell (d) of Table IV: 2 optimal points $\in \{(-48^\circ, 48^\circ), (48^\circ, -48^\circ)\}$ | Table cell (e) of Table IV: 1 optimal point $\in \{(32^\circ, 32^\circ)\}$ | Table cell (f) of Table IV: 2 optimal points $\in \{(-26^\circ, 35^\circ), (35^\circ, -26^\circ)\}$ |
| | $f(\theta_1^*, \theta_2^*)$ | 51.0780 | 34.3548 | 81.2773 |
| | Δ_2 | 0.3918 | 0 | 0.0757 |
| $G > C$ | (θ_1^*, θ_2^*) | Table cell (g) of Table IV: 2 optimal points $\in \{(-69^\circ, 69^\circ), (69^\circ, -69^\circ)\}$ | Table cell (h) of Table IV: 1 optimal point $\in \{(59^\circ, 59^\circ)\}$ | Table cell (i) of Table IV: 2 optimal points $\in \{(-90^\circ, 90^\circ), (90^\circ, -90^\circ)\}$ |
| | $f(\theta_1^*, \theta_2^*)$ | 42.7376 | 10.0621 | 57.2246 |
| | Δ_2 | 1.0154 | 0 | 0.5424 |
| $G \gg C$ | (θ_1^*, θ_2^*) | Table cell (j) of Table IV: 2 optimal points $\in \{(-90^\circ, 90^\circ), (90^\circ, -90^\circ)\}$ | Table cell (k) of Table IV: 1 optimal point $\in \{(90^\circ, 90^\circ)\}$ | Table cell (l) of Table IV: 1 optimal point $\in \{(-90^\circ, -90^\circ)\}$ |
| | $f(\theta_1^*, \theta_2^*)$ | 27.8739 | 1.2400 | 26.1165 |
| | Δ_2 | 2.0891 | 0 | 0 |

Table VIII:
SUMMARY OF ALL OPTIMAL ORIENTATION ANGLES FOR 3 PV CELLS WITH THE DIFFERENT LOAD PROFILES FROM TABLE V

| | | Constant Load Profile | Business Load Profile | Residential Load Profile |
|-----------|---|---|---|--|
| $G \ll C$ | $(\theta_1^*, \theta_2^*, \theta_3^*)$ | Table cell (a) of Table V: 1 optimal point $\in \{(0^\circ, 0^\circ, 0^\circ)\}$ | Table cell (b) of Table V: 1 optimal point $\in \{(0^\circ, 0^\circ, 0^\circ)\}$ | Table cell (c) of Table V: 1 optimal point $\in \{(0^\circ, 0^\circ, 0^\circ)\}$ |
| | $f(\theta_1^*, \theta_2^*, \theta_3^*)$ | 60.0712 | 101.3440 | 100.2310 |
| | Δ_3 | 0 | 0 | 0 |
| $G < C$ | $(\theta_1^*, \theta_2^*, \theta_3^*)$ | Table cell (d) of Table V: 6 optimal points $\in \{(-55^\circ, 42^\circ, 42^\circ), (-42^\circ, -42^\circ, 55^\circ), (-42^\circ, 55^\circ, -42^\circ), (42^\circ, -55^\circ, 42^\circ), (42^\circ, 42^\circ, -55^\circ), (55^\circ, -42^\circ, -42^\circ)\}$ | Table cell (e) of Table V: 1 optimal point $\in \{(32^\circ, 32^\circ, 32^\circ)\}$ | Table cell (f) of Table V: 3 optimal points $\in \{(-33^\circ, 31^\circ, 31^\circ), (31^\circ, -33^\circ, 31^\circ), (31^\circ, 31^\circ, -33^\circ)\}$ |
| | $f(\theta_1^*, \theta_2^*, \theta_3^*)$ | 51.1204 | 34.3548 | 81.2783 |
| | Δ_3 | -0.0424 | 0 | -0.001 |
| $G > C$ | $(\theta_1^*, \theta_2^*, \theta_3^*)$ | Table cell (g) of Table V: 6 optimal points $\in \{(-76^\circ, 60^\circ, 60^\circ), (-60^\circ, -60^\circ, 76^\circ), (-60^\circ, 76^\circ, -60^\circ), (60^\circ, -76^\circ, 60^\circ), (60^\circ, 60^\circ, -76^\circ), (76^\circ, -60^\circ, -60^\circ)\}$ | Table cell (h) of Table V: 1 optimal point $\in \{(59^\circ, 59^\circ, 59^\circ)\}$ | Table cell (i) of Table V: 3 optimal points $\in \{(-85^\circ, -85^\circ, 87^\circ), (-85^\circ, 87^\circ, -85^\circ), (87^\circ, -85^\circ, -85^\circ)\}$ |
| | $f(\theta_1^*, \theta_2^*, \theta_3^*)$ | 42.8827 | 10.0621 | 57.2542 |
| | Δ_3 | -0.1451 | 0 | -0.0296 |
| $G >> C$ | $(\theta_1^*, \theta_2^*, \theta_3^*)$ | Table cell (j) of Table V: 6 optimal points $\in \{(-90^\circ, -90^\circ, 90^\circ), (-90^\circ, 90^\circ, -90^\circ), (-90^\circ, 90^\circ, 90^\circ), (90^\circ, -90^\circ, -90^\circ), (90^\circ, -90^\circ, 90^\circ), (90^\circ, 90^\circ, -90^\circ)\}$ | Table cell (k) of Table V: 1 optimal point $\in \{(90^\circ, 90^\circ, 90^\circ)\}$ | Table cell (l) of Table V: 3 optimal points $\in \{(-90^\circ, -90^\circ, 90^\circ), (-90^\circ, 90^\circ, -90^\circ), (90^\circ, -90^\circ, -90^\circ)\}$ |
| | $f(\theta_1^*, \theta_2^*, \theta_3^*)$ | 28.2100 | 1.2400 | 25.9671 |
| | Δ_3 | -0.3361 | 0 | 0.1494 |